Journal of Sound and Vibration 329 (2010) 4515–4533

Contents lists available at ScienceDirect

Journal of Sound and Vibration

journal homepage: www.elsevier.com/locate/jsvi

Generalised modal stability of inclined cables subjected to support excitations

J.H.G. Macdonald *, M.S. Dietz, S.A. Neild, A. Gonzalez-Buelga, A.J. Crewe, D.J. Wagg

Faculty of Engineering, University of Bristol, Queen's Building, University Walk, Bristol BS8 1TR, UK

ARTICLE INFO

Article history:
Received 28 October 2009
Received in revised form
7 April 2010
Accepted 6 May 2010
Handling Editor: M.P. Cartmell
Available online 23 May 2010

ABSTRACT

Parametric excitation is of concern for cables such as on cable-stayed bridges, whereby small amplitude end motion can lead to large, potentially damaging, cable vibrations. Previous identification of the stability boundaries for the onset of such vibrations has considered only a single mode of the cable, ignoring non-linear coupling between modes, or has been limited to special cases. Here multiple cable modes in both planes are included, with support excitation close to any natural frequency. Cable inclination, sag, parametric and direct excitation and nonlinearities, including modal coupling, are included. The only significant limitation is that the sag is small. The method of scaling and averaging is used to find the steady-state amplitude of the directly excited mode and, in the presence of this response, to define stability boundaries of other modes excited parametrically or through nonlinear modal coupling. It is found that the directly excited response significantly modifies the stability boundaries compared to previous simplified solutions. The analysis is validated by a series of experimental tests, which also identified another nonlinear mechanism which caused significant cable vibrations at twice the excitation frequency in certain conditions. This new mechanism is explained through a refinement of the analysis.

1. Introduction

Inclined cables are important structural elements on cable-stayed bridges and guyed masts. Large cable vibrations have been observed on several major bridges and although aerodynamic effects are sometimes responsible, another source of excitation of concern comes from motion of the deck and/or tower. The natural frequencies of local cable vibrations and global structural vibrations are generally in the same frequency range, leading to potential dynamic interactions. These, along with nonlinear effects, can produce complex behaviour involving large amplitude cable vibrations; see for example the reviews by Nayfeh and Pai [1], Rega [2,3] and Ibrahim [4].

Of particular concern is parametric excitation, whereby small amplitude deck/tower motions with a component along the cable axis can cause large amplitude cable motions at half the excitation frequency [5]. These vibrations can occur in-plane (defined as the plane in which the cable sags statically) or out-of-plane, even if the anchorage motion is limited to in-plane, which is generally the dominant direction of deck motion on cable-stayed bridges. This paper aims to identify the conditions under which modal vibrations of a cable become unstable about the zero response, in which case large vibrations in the mode could arise, potentially leading to damage. Parametric excitation is one mechanism by which such

* Corresponding author. Tel.: +44 117 331 5735; fax: +44 117 331 5719.
E-mail addresses: john.macdonald@bristol.ac.uk (J.H.G. Macdonald), m.dietz@bristol.ac.uk (M.S. Dietz), simon.neild@bristol.ac.uk (S.A. Neild), aliciagbuelga@yahoo.es (A. Gonzalez-Buelga), a.j.crewe@bristol.ac.uk (A.J. Crewe), david.wagg@bristol.ac.uk (D.J. Wagg).

0022-460X/$ - see front matter © 2010 Elsevier Ltd. All rights reserved.
doi:10.1016/j.jsv.2010.05.002

an instability can occur. For inclined cables subject to vertical deck motion and/or horizontal tower motion, the situation is complicated by the existence of simultaneous direct (external) and parametric excitations.

Analysis of parametric excitation of cables has often been based on the Mathieu–Hill equation for a single mode [5–7] neglecting nonlinear coupling between modes. On this basis Lilien and Pinto da Costa [5] provide the following expression for the minimum axial support amplitude required to cause parametric excitation in the first mode:

$$U_{crit} = 2\varepsilon_s L \sqrt{\left[1-\left(\frac{\Omega}{2\omega_1}\right)^2\right]^2 + 4\xi_1^2\left[\frac{\Omega}{2\omega_1}\right]^2}, \tag{1}$$

where ε_s is the static strain, L the cable length, Ω the excitation frequency and ω_1 and ξ_1 the natural frequency and damping ratio of the first mode, where $\Omega/2\omega_1 \approx 1$. An equivalent expression (for $\Omega/2\omega_1 \approx 1$) is given in the SETRA guidelines [8], which are in common use for stay cable design. The expression can be applied to other cable modes by substituting the relevant natural frequency and damping ratio.

Uhrig [7] included nonlinear coupling and parametric excitation terms in his derivation of the equations governing in-plane vibrations of an inclined cable with horizontal input at the upper anchorage. However, he reduced them to uncoupled linear Mathieu equations to consider the solution. Caetano [9] considered end motion axially and transversely to the cable, but treated them as separate cases.

Perkins [10] addressed tangential support motion of a sagging cable, providing simultaneous principal parametric excitation of the first out-of-plane mode and external excitation of the first (symmetric) in-plane mode (with twice the natural frequency, due to the sag). The cable was modelled as a coupled two-degree-of-freedom (2DOF) system and experiments exhibited similar behaviour to that predicted. Zhang and Tang [11] also considered a 2DOF cable model subjected to tangential support motion, in this case with 1:1 internal resonance between the in-plane and out-of-plane modes and excitation around twice the natural frequency. Hence, although there was external excitation of the in-plane mode (if symmetric), it was far from the mode's natural frequency.

A number of authors have considered an inclined cable subject to vertical support excitation of the lower anchorage, including parametric excitation and nonlinear terms. Berlioz and Lamarque [12] used the multiple scales method to estimate the response amplitudes of a 1DOF model of the first in-plane mode (detuned from other modes by the sag), subject to excitation around its natural frequency (direct excitation) or at twice the natural frequency (parametric excitation). After fitting parameters good agreement with experiments was found. Georgakis and Taylor [13,14] explored the responses of a cable modelled with four shape functions, subjected to both sinusoidal and stochastic support excitations, by extensive numerical simulations. Wang and Zhao [15] obtained numerical results of amplitudes of planar and non-planar responses for certain cases, from the shooting method and the continuation technique. Pinto da Costa et al. [16] discussed the relative importance of direct and parametric excitation of inclined cables, by analytically considering horizontal and vertical cables and from numerical solutions of vibration amplitudes of four different inclined cables. Chai and Chen [17] conducted numerical simulations of the in-plane response of the equivalent system of inclined guy cables to horizontal sinusoidal motion of the upper anchorage. Nayfeh et al. [18] analysed a vertical cable (i.e. with no sag) with inclined excitation. The method of multiple scales and numerical solution of the resulting modulation equations were used to predict amplitudes of steady-state motion for certain parameter values, in good agreement with experiments. All of these studies focussed on the amplitudes of the responses, inevitably resorting to some numerical technique using certain parameter values.

Other studies have considered autoparametric resonance of an inclined cable interacting with a beam, including nonlinearities, but only including a single in-plane mode of the cable (or cable-dominated mode of the combined system) [19–21]. An alternative cable-deck model proposed by Georgakis et al. [14,22] and developed by Lorenzo [23] allows for autoparametric resonance and nonlinearities and includes multiple cable modes, but has only been solved by numerical simulation.

For a cable with small sag, the natural frequencies are close to commensurate [24]. Hence for primary parametric excitation of any one mode (at twice its natural frequency), the excitation frequency is close to the natural frequency of another mode. Therefore, inputs at an angle to the cable axis (e.g. vertical anchorage motion on an inclined cable) can cause simultaneous direct excitation and parametric excitation of at least two modes, which are nonlinearly coupled [16]. Due to the coupling, the response of the directly excited mode can modify the dynamic stability of other modes. The effect on the stability boundaries had not been considered until recently [25], when a three-degree-of-freedom model, with 1:2:2 frequency ratios, was used for vertical excitation of the lower anchorage of an inclined cable excited around the natural frequency of the second in-plane mode. Stability boundaries for the first and second out-of-plane modes were identified analytically.

Here this analysis has been generalised to include all in-plane and out-of-plane modes, for excitation close to any natural frequency. The cable inclination, sag, parametric and direct excitation and nonlinearities, including modal coupling, are all included. The only significant limitation is that the sag is small.

For inputs of low amplitude or away from critical frequencies it is found that the cable essentially responds only in the directly excited mode, although the amplitude is significantly affected by nonlinearities. The zero amplitude response stability boundaries of other modes are derived analytically using the method of scaling and averaging. For input

amplitudes above these boundaries parametric excitation and nonlinear coupling between modes initiate oscillations in modes other than the directly excited mode, which could lead to damaging large amplitude responses.

The theoretical stability boundaries are validated though a series of experimental tests. These tests also unveiled another nonlinear mechanism causing significant cable vibrations at twice the excitation frequency in certain conditions. A refinement of the analysis is able to explain this effect, also caused by the simultaneous axial and transverse excitation of the cable.

2. Derivation of theoretical stability boundaries

2.1. Equations of motion

There have been many representations of the equations of motion for cables [1]. In this paper the modal equations derived by Warnitchai et al. [26] are adopted. These equations are valid for elastic inclined cables with small sag, they include cubic and quadratic nonlinearities, and they allow for small support motions in all directions at both ends of the cable. They are therefore very appropriate for the taut inclined cables considered here. The cable is supported at end points a and b and the direction of the chord line from a to b is defined as x (Fig. 1). The static sag profile lies in the x–z plane, so z represents in-plane motion and y represents out-of-plane motion. The angle of inclination of the chord relative to the horizontal is defined as θ. Axial vibrations of the cable are neglected since they occur at a much higher frequency than transverse vibrations. The equation of motion of the nth out-of-plane cable mode is expressed as [26]

$$\begin{aligned} &m_{yn}(\ddot{y}_n+2\xi_{yn}\omega_{yn}\dot{y}_n+\omega_{yn}^2 y_n)+\textstyle\sum_k v_{nk}y_n(y_k^2+z_k^2)+\sum_k 2\beta_{nk}y_n z_k \\ &\quad+2\eta_n(u_b-u_a)y_n+\zeta_n(\ddot{v}_a+(-1)^{n+1}\ddot{v}_b)=F_{yn}, \end{aligned} \tag{2}$$

and that of the nth in-plane cable mode as

$$\begin{aligned} &m_{zn}(\ddot{z}_n+2\xi_{zn}\omega_{zn}\dot{z}_n+\omega_{zn}^2 z_n)+\textstyle\sum_k v_{nk}z_n(y_k^2+z_k^2)+\sum_k 2\beta_{nk}z_n z_k \\ &+\textstyle\sum_k \beta_{kn}(y_k^2+z_k^2)+2\eta_n(u_b-u_a)z_n+\zeta_n(\ddot{w}_a+(-1)^{n+1}\ddot{w}_b)-\alpha_n(\ddot{u}_b-\ddot{u}_a)=F_{zn}, \end{aligned} \tag{3}$$

where y_n and z_n are the generalised displacements of the cable in the nth out-of-plane and in-plane modes, respectively, for any n (note that the summations over modes y_k and z_k, for all k, cause nonlinear coupling between modes); subscripts a and b denote the top and bottom anchorage points, respectively, and the modal masses m_{yn} and m_{zn} and the parameters v_{nk}, β_{nk}, η_n, ζ_n and α_n are given by

$$m_{yn}=m_{zn}=m=\frac{\rho AL}{2}, \quad v_{nk}=\frac{EA\pi^4 n^2 k^2}{8L^3},$$

$$\beta_{nk}=\frac{EA\pi\gamma n^2}{4L\sigma_s}\left(\frac{1+(-1)^{k+1}}{k}\right), \quad \eta_n=\frac{E_q A\pi^2 n^2}{4L^2},$$

$$\zeta_n=\frac{\rho AL}{n\pi}, \quad \alpha_n=\frac{\rho AL}{n^3\pi^3}\frac{\gamma LE_q}{\sigma_s^2}(1+(-1)^{n+1}),$$

where ρ is the density, A the cross sectional area, L the chord length, E the Young's Modulus and σ_s the static stress.

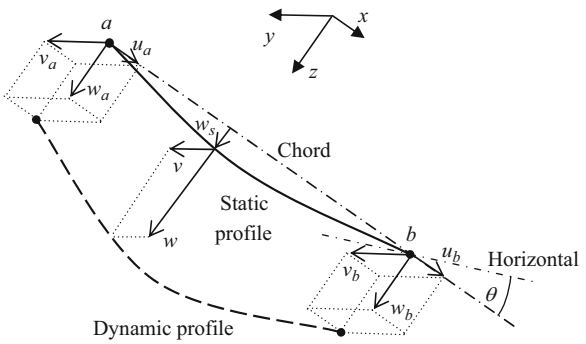

Fig. 1. Definition of cable coordinate system.

Ernst's equivalent modulus of the cable, E_q [27], Irvine's non-dimensional sag parameter, λ^2 [24], and the component of weight normal to the cable axis, γ, are given by

$$E_q = \frac{E}{1+\lambda^2/12}, \quad \lambda^2 = \frac{E}{\sigma_s}\left(\frac{\gamma L}{\sigma_s}\right)^2, \quad \gamma = \rho g \cos\theta,$$

where g is the gravitational acceleration.

The out-of-plane and in-plane natural frequencies, ω_{yn} and $\omega_{zn,}$ respectively, are given by

$$\omega_{yn} = \frac{n\pi}{L}\sqrt{\frac{\sigma_s}{\rho}}, \quad \omega_{zn} \approx \frac{n\pi}{L}\sqrt{\frac{\sigma_s}{\rho}(1+k_n)},$$

where $k_n = \left(\frac{2\lambda^2}{\pi^4 n^4}\right)(1+(-1)^{n+1})^2$.

F_{yn} and F_{zn} are the generalised external loads on the cable in each mode and it is assumed that damping can be modelled as viscous with modal damping ratios ξ_{zn} and ξ_{yn}. Details of the derivation are given by Warnitchai et al. [26].

Noting that for cables with small sag $k_n \ll 1$, the natural frequencies can alternatively be represented by

$$\omega_{yn} = \omega_n = n\omega_1, \quad \omega_{zn} \approx \omega_n(1+\kappa_n),$$

where

$$\omega_1 = \frac{\pi}{L}\sqrt{\frac{\sigma_s}{\rho}} \text{ and } \kappa_n = \left(\frac{\lambda^2}{\pi^4 n^4}\right)(1+(-1)^{n+1})^2. \tag{4}$$

In Eqs. (2) and (3), the m_{yn} and m_{zn} terms are linear, the v_{nk} terms are cubic nonlinearities from stretching of the cable in the deformed shape, the β_{nk} terms are quadratic nonlinearities from the effect of the static sag, the η_n terms cause parametric excitation from the axial end displacements and the ζ_n and α_n terms cause direct excitation from the end accelerations. The equations of motion of all modes are coupled through the nonlinear terms.

This paper focuses on the response to support motions, with no external forces applied along the length of the cable ($F_{yn}=F_{zn}=0$). For conciseness the support motions are expressed as

$$u = u_b - u_a, \quad v_n = v_a + (-1)^{n+1} v_b, \quad w_n = w_a + (-1)^{n+1} w_b.$$

It is assumed here that the rest of the structure to which the cable is attached is not affected by the dynamics of the cable. The cable is excited by prescribed sinusoidal support motions (which in general can be a combination of u, v_n and w_n components) close to the pth natural frequency, with excitation frequency

$$\Omega = p\omega_1(1+\mu), \tag{5}$$

where μ is a small frequency detuning parameter. Hence p is the mode number of the modes (one in each plane, y_p and z_p) with natural frequencies close to the excitation frequency, whereas n is the mode number of any mode under consideration.

2.2. Scaling and averaging

The method of scaling and averaging [28] is applied to the equations of motion to determine the steady-state amplitudes of directly excited modes and the dynamic stability of other modes. Wagg and Neild [29] made a comparison with the method of multiple scales to calculate the response of mode z_2 in the absence of any other modal responses. The results were found to be the same (to order ε), but the analysis using the method of scaling and averaging was somewhat simpler so it is adopted here to address the multiple mode case.

Time is transformed using the relationship $\tau = (1+\mu)t$ and the small parameter ε is introduced for book-keeping purposes. Hence Eqs. (2) and (3) are scaled such that they are in standard Lagrange form [30,31]

$$y_n'' + \omega_n^2 y_n = \varepsilon X_{yn} + O(\varepsilon^2), \quad z_n'' + \omega_n^2 z_n = \varepsilon X_{zn} + O(\varepsilon^2), \tag{6}$$

where {}' represents differentiation with respect to τ and

$$X_{yn} = 2\mu\omega_n^2 y_n - 2\xi_{yn}\omega_n y_n' - \sum_k \frac{v_{nk}}{m} y_n(y_k^2+z_k^2) - \sum_k \frac{2\beta_{nk}}{m} y_n z_k - \frac{2\eta_n}{m} u y_n - \frac{\zeta_n}{m} v_n'', \tag{7}$$

$$\begin{aligned} X_{zn} = {} & 2\mu\omega_n^2 z_n - 2\xi_{zn}\omega_n z_n' - 2\kappa_n\omega_n^2 z_n - \textstyle\sum_k \frac{v_{nk}}{m} z_n(y_k^2+z_k^2) - \sum_k \frac{2\beta_{nk}}{m} z_n z_k \\ & - \textstyle\sum_k \frac{\beta_{kn}}{m}(y_k^2+z_k^2) - \frac{2\eta_n}{m} u z_n - \frac{\zeta_n}{m} w_n'' + \frac{\alpha_n}{m} u''. \end{aligned} \tag{8}$$

The form of Eqs. (6) reflects the fact that the response of each mode is dominated by its linear undamped response. The $O(\varepsilon^2)$ and higher order terms are neglected.

The equations are now in a form that can be averaged [28,30,31]. A trial solution of Eqs. (6) is proposed with the form

$$y_n = y_{nc}\cos(\omega_n\tau)+y_{ns}\sin(\omega_n\tau). \tag{9}$$

Substituting this into the left hand side of the equation it can be shown that a solution exists with

$$y'_{nc} = -\frac{\varepsilon}{\omega_n}\sin(\omega_n\tau)X_{yn}, \quad y'_{ns} = \frac{\varepsilon}{\omega_n}\cos(\omega_n\tau)X_{yn}, \tag{10}$$

and

$$y'_n = -\omega_n y_{nc}\sin(\omega_n\tau)+\omega_n y_{ns}\cos(\omega_n\tau), \tag{11}$$

(and similarly for z_n).

Eqs. (10) can be averaged by integrating with respect to τ over the fundamental period $\tau_1=2\pi/\omega_1$ (i.e. in terms of real time, p times the excitation period, $t_1=2\pi p/\Omega$). Since, also from Eqs. (10), the derivatives of y_{nc} and y_{ns} (and z_{nc} and z_{ns}) are small, these amplitudes may be treated as constant over the integration period [30]. In the integration, only the components of X_{yn} (or X_{zn}) at frequency ω_n (with respect to τ) give non-zero terms. The resulting averaged derivatives of the amplitudes, represented with an additional subscript a, are

$$y'_{nca} = -\frac{\varepsilon}{\omega_n}\left\{\xi_{yn}\omega_n^2 y_{nca}+\mu\omega_n^2 y_{nsa}-\frac{\nu_{nn}}{8m}y_{nsa}(Y_{na}^2-Z_{na}^2)-\sum_k\frac{\nu_{nk}}{4m}y_{nsa}(Y_{ka}^2+Z_{ka}^2)-\frac{\nu_{nn}}{4m}z_{nsa}C_{na}+\delta_{2n,p}\frac{\eta_n}{2m}Uy_{nsa}\right\}, \tag{12}$$

$$y'_{nsa} = \frac{\varepsilon}{\omega_n}\left\{-\xi_{yn}\omega_n^2 y_{nsa}+\mu\omega_n^2 y_{nca}-\frac{\nu_{nn}}{8m}y_{nca}(Y_{na}^2-Z_{na}^2)-\sum_k\frac{\nu_{nk}}{4m}y_{nca}(Y_{ka}^2+Z_{ka}^2)-\frac{\nu_{nn}}{4m}z_{nca}C_{na}-\delta_{2n,p}\frac{\eta_n}{2m}Uy_{nca}+\delta_{n,p}\frac{\omega_n^2}{2m}\zeta_n V_n\right\}, \tag{13}$$

$$z'_{nca} = -\frac{\varepsilon}{\omega_n}\left\{\xi_{zn}\omega_n^2 z_{nca}+(\mu-\kappa_n)\omega_n^2 z_{nsa}-\frac{\nu_{nn}}{8m}z_{nsa}(Z_{na}^2-Y_{na}^2)-\sum_k\frac{\nu_{nk}}{4m}z_{nsa}(Z_{ka}^2+Y_{ka}^2)-\frac{\nu_{nn}}{4m}y_{nsa}C_{na}+\delta_{2n,p}\frac{\eta_n}{2m}Uz_{nsa}\right\}, \tag{14}$$

$$z'_{nsa} = \frac{\varepsilon}{\omega_n}\left\{-\xi_{zn}\omega_n^2 z_{nsa}+(\mu-\kappa_n)\omega_n^2 z_{nca}-\frac{\nu_{nn}}{8m}z_{nca}(Z_{na}^2-Y_{na}^2)-\sum_k\frac{\nu_{nk}}{4m}z_{nca}(Z_{ka}^2+Y_{ka}^2)-\frac{\nu_{nn}}{4m}y_{nca}C_{na}-\delta_{2n,p}\frac{\eta_n}{2m}Uz_{nca}+\delta_{n,p}\frac{\omega_n^2}{2m}(\zeta_n W_n-\alpha_n U)\right\}, \tag{15}$$

where $Y_{na}^2=y_{nca}^2+y_{nsa}^2$ and $Z_{na}^2=z_{nca}^2+z_{nsa}^2$ are squares of the modal amplitudes, $C_{na}=y_{nca}z_{nca}+y_{nsa}z_{nsa}$ are cross-coupling terms, $\delta_{i,j}$ is the Kronecker delta function and U, V_n and W_n are the amplitudes of the sinusoidal support motions u, v_n and w_n.

The averaged equations for the y and z components are identical except all occurrences of y and z are exchanged and in the z equations μ is replaced by $(\mu-\kappa_n)$ and $\zeta_n V_n$ by $(\zeta_n W_n-\alpha_n U)$. Both of these latter effects are due to the static sag of the cable, although for even n, κ_n and α_n are both equal to zero so these differences do not exist.

2.3. Direct excitation

For all modal responses starting with zero amplitude, the only non-zero rates of amplitude increase are for y'_{psa} and z'_{psa}. i.e. only modes y_p and z_p, with natural frequencies close to the excitation frequency, are directly excited.

For pure out-of-plane excitation ($W_p=U=0$), for a response only in mode y_p (the stability of other modes is considered below), the rates of amplitude increase are

$$y'_{pca} = -\frac{\varepsilon}{\omega_n}\left\{\xi_{yp}\omega_p^2 y_{pca}+\mu\omega_p^2 y_{psa}-\frac{3\nu_{pp}}{8m}y_{psa}Y_{pa}^2\right\}, \tag{16}$$

$$y'_{psa} = \frac{\varepsilon}{\omega_n}\left\{-\xi_{yp}\omega_p^2 y_{psa}+\mu\omega_p^2 y_{pca}-\frac{3\nu_{pp}}{8m}y_{pca}Y_{pa}^2+\frac{\zeta_p}{2m}\omega_p^2 V_p\right\}. \tag{17}$$

Setting these both to zero leads to the following equation that defines the steady-state amplitude in mode y_p (Y_{pa})

$$9\nu_{pp}^2 Y_{pa}^6-48m\omega_p^2\mu\nu_{pp}Y_{pa}^4+64m^2\omega_p^4(\mu^2+\xi_{yp}^2)Y_{pa}^2=16\omega_p^4\zeta_p^2 V_p^2. \tag{18}$$

Similarly, for in-plane excitation ($V_p=0$), the steady-state amplitude of mode z_p (Z_{pa}) (in the absence of any other modal responses) is given by

$$9\nu_{pp}^2 Z_{pa}^6-48m\omega_p^2(\mu-\kappa_p)\nu_{pp}Z_{pa}^4+64m^2\omega_p^4\left\{(\mu-\kappa_p)^2+\xi_{zp}^2\right\}Z_{pa}^2=16\omega_p^4(\zeta_p W_p-\alpha_p U)^2. \tag{19}$$

Hence Eqs. (18) and (19) are cubic equations in Y_{pa}^2 and Z_{pa}^2, respectively, which for given cable and excitation parameters can be solved to find the steady-state amplitude in the directly excited mode. If the first two terms on the left hand side are neglected, Eq. (18) agrees with conventional linear analysis (for small μ). For sufficiently small amplitudes this is valid, but in general the first two nonlinear terms express the dynamic stiffening that causes the resonance curve to bend over

towards higher frequencies. It is noteworthy that in Eq. (19) the effective input amplitude is reduced by $\alpha_p U$. Hence, the axial component of end motion, which is often neglected when considering direct excitation, can have a significant effect on the response amplitude of odd in-plane modes.

2.4. Modal stability

Due to the parametric excitation and nonlinear coupling terms in the equations of motion, the zero amplitude response solution of other modes can become dynamically unstable. The localised stability of mode n is considered, around the semi-trivial solution having zero response in this mode along with the directly excited response in mode p, above. Loss of stability of this solution indicates that a response in mode n will occur.

For all modes other than the directly excited mode(s), the first order differential equations, Eqs. (12) and (13), can be expressed in matrix form (with no loss of generality) as

$$\begin{Bmatrix} y'_{nca} \\ y'_{nsa} \end{Bmatrix} = \begin{bmatrix} c_{11} & c_{12} \\ c_{21} & c_{22} \end{bmatrix} \begin{Bmatrix} y_{nca} \\ y_{nsa} \end{Bmatrix}, \tag{20}$$

(and similarly for in-plane modes from Eqs. (14) and (15)).

The eigenvalues, χ, are then given by the solution of the characteristic equation

$$\chi^2 - (c_{11}+c_{22})\chi + c_{11}c_{22} - c_{12}c_{21} = 0. \tag{21}$$

On the local stability boundary the larger real part of the two eigenvalues is zero, hence

$$c_{11}c_{22} - c_{12}c_{21} = 0. \tag{22}$$

For pure out-of-plane or in-plane excitation, only mode y_p or z_p, respectively, is directly excited. For the localised stability of each other mode about zero response, it is sufficient to only retain the linear terms in that mode and it is assumed that all other modes, apart from the directly excited one, have zero amplitude.

For direct excitation of mode z_p (with $V_p=0$), the matrix in Eq. (20), for mode y_n, with $n \neq p$, then becomes

$$\begin{bmatrix} c_{11} & c_{12} \\ c_{21} & c_{22} \end{bmatrix} = \frac{\varepsilon}{\omega_n} \begin{bmatrix} -\xi_{yn}\omega_n^2 & -\mu\omega_n^2 + \dfrac{\nu_{np}}{4m} Z_{pa}^2 - \delta_{2n,p} \dfrac{\eta_n}{2m} U \\ \mu\omega_n^2 - \dfrac{\nu_{np}}{4m} Z_{pa}^2 - \delta_{2n,p} \dfrac{\eta_n}{2m} U & -\xi_{yn}\omega_n^2 \end{bmatrix}, \tag{23}$$

hence, from Eq. (22), the local stability boundary is given by

$$\xi_{yn}^2 \omega_n^4 + \left(\mu\omega_n^2 - \frac{\nu_{np}}{4m} Z_{pa}^2\right)^2 - \delta_{2n,p} \left(\frac{\eta_n}{2m}\right)^2 U^2 = 0. \tag{24}$$

For $2n \neq p$ (and $n \neq p$) there are no real solutions and mode y_n (for all other n) is always stable about the zero response, for any amplitude of mode z_p. Similarly, for $2n \neq p$ (and $n \neq p$), mode z_n is always stable. Equivalent conditions exist in the presence of direct excitation of mode y_p (with $W_p = U = 0$), except modes y_n and z_n are also stable for $2n = p$. Therefore, during direct excitation of any one mode (y_p or z_p), all other modes are always stable about the zero solution, except for the mode in the other plane at the same frequency (mode z_p or y_p, respectively) and, for in-plane excitation with an axial component of end motion, the modes in both planes at half the excitation frequency (modes y_q and z_q, where $q = p/2$). Considering these exceptions, for example, in-plane excitation close to $2\omega_1$ results in direct excitation of mode z_2 and can, for certain ranges of excitation frequency and amplitude, trigger motion in modes y_2, y_1 or z_1. The trigger conditions for the modes at half the excitation frequency and for the mode in the other plane at the excitation frequency are addressed in the next two sub-sections.

2.5. Parametric excitation

For $2n = p$ (i.e. for excitation frequency $\Omega \approx 2\omega_q$, where $q = n = p/2$), from Eq. (24) the stability boundary of mode y_q becomes

$$\nu_{qp}^2 Z_{pa}^4 - 8m\mu\omega_q^2 \nu_{qp} Z_{pa}^2 + 16m^2\omega_q^4(\mu^2 + \xi_{yq}^2) = 4\eta_q^2 U^2. \tag{25}$$

Hence for an axial component of cable end motion, U, larger than given by this expression, mode y_q, at half the excitation frequency, becomes unstable due to parametric excitation. There is an identical expression for the stability boundary for parametric excitation of mode z_q, except ξ_{yq} is replaced by ξ_{zq} and μ by $(\mu - \kappa_q)$.

In the absence of a direct response in mode z_p ($Z_{pa}=0$), the stability boundary in Eq. (25) equals (to first order ε) the boundaries given by Lilien and Pinto da Costa [5] and SETRA [8]. In the case of pure axial excitation ($V_p = W_p = 0$), since for integer q, p is even, so $\alpha_p = 0$, from Eq. (19) the only real solution for the steady-state response of mode z_p is $Z_{pa}=0$. Hence in this case, the stability boundaries from Lilien and Pinto da Costa and SETRA are valid. However, in the more general case the axial excitation is accompanied by a transverse component of end motion ($W_p \neq 0$), which gives a non-zero response of mode z_p, which modifies the stability boundary in accordance with Eq. (25). The effect of the response in mode z_p is effectively to increase the mean tension in the cable, thus shifting the parametric stability boundary of mode y_q (and mode z_q) to higher frequencies.

2.6. Nonlinear modal coupling between modes in orthogonal planes

For direct excitation of mode z_p (with V_p=0), the matrix in Eq. (20), for mode y_p (n=p) becomes

$$\begin{bmatrix} c_{11} & c_{12} \\ c_{21} & c_{22} \end{bmatrix} = \frac{\varepsilon}{\omega_n} \begin{bmatrix} -\xi_{yp}\omega_p^2 + \dfrac{v_{pp}}{4m} z_{psa} z_{pca} & -\mu\omega_p^2 + \dfrac{v_{pp}}{8m}(Z_{pa}^2 + 2z_{psa}^2) \\ \mu\omega_p^2 - \dfrac{v_{pp}}{8m}(Z_{pa}^2 + 2z_{pca}^2) & -\xi_{yp}\omega_p^2 - \dfrac{v_{pp}}{4m} z_{psa} z_{pca} \end{bmatrix}, \tag{26}$$

hence, from Eq. (22), the local stability boundary is given by

$$3v_{pp}^2 Z_{pa}^4 - 32m\mu\omega_p^2 v_{pp} Z_{pa}^2 + 64m^2\omega_p^4(\mu^2 + \xi_{yp}^2) = 0. \tag{27}$$

For given detuning, μ, within a certain range, there are two positive solutions for Z_{pa}. Mode y_p is unstable between these two solutions, hence the (planar) response in mode z_p cannot be sustained alone and the total response involves motion both in-plane and out-of-plane, although the excitation is only in-plane. This type of response is discussed by Nayfeh and Mook [32] and was investigated numerically and experimentally by Nayfeh et al. [18].

Similarly, for direct excitation of mode y_p (with W_p=U=0), there is an equivalent stability boundary for mode z_p, with ξ_{yp} replaced by ξ_{zp}, μ by $(\mu-\kappa_p)$ and Z_{pa} by Y_{pa}.

2.7. Non-dimensional response and stability boundaries

For direct excitation of any one mode, the steady-state response of that mode, up to the stability boundary of any other mode, is given by Eq. (18) or (19). The stability boundary of the corresponding mode in the other plane is given by Eq. (27) (or the equivalent for direct excitation of mode y_p and stability of mode z_p). For direct excitation of an even in-plane mode with a component of axial end motion, the stability boundaries for parametric excitation of the modes with nominally half the natural frequency are given by Eq. (25) for the out-of-plane mode and an equivalent equation for the in-plane mode. Hence these few equations govern the generalised modal stability of the cable.

For general application and to relate full-scale behaviour and laboratory experiments, these equations are re-expressed in non-dimensional form. The input and output displacements are non-dimensionalised with respect to L: $\hat{U} = U/L$, $\hat{Y}_{pa} = Y_{pa}/L$, etc., and two non-dimensional cable parameters are defined: ε_s=σ_s/E (i.e. static strain) and Γ=$\rho g L/\sigma_s$ (i.e. ratio of cable weight to tension). Irvine's non-dimensional sag parameter can then be expressed as λ^2=$\Gamma^2\cos^2\theta/\varepsilon_s$.

Eq. (18), for the steady-state out-of-plane response in mode y_p (for W_p=U=0), then becomes

$$9(\hat{Y}_{pa}p\pi)^6 - 192\varepsilon_s\mu(\hat{Y}_{pa}p\pi)^4 + 1024\varepsilon_s^2(\mu^2 + \xi_{yp}^2)(\hat{Y}_{pa}p\pi)^2 = 1024\varepsilon_s^2\hat{V}_p^2 \tag{28}$$

and Eq. (19) for the steady-state in-plane response in mode z_p (for V_p=0), becomes

$$\begin{aligned} &9(\hat{Z}_{pa}p\pi)^6 - 192\varepsilon_s(\mu-\kappa_p)(\hat{Z}_{pa}p\pi)^4 + 1024\varepsilon_s^2\left((\mu-\kappa_p)^2 + \xi_{zp}^2\right)(\hat{Z}_{pa}p\pi)^2 \\ &\quad = 1024\varepsilon_s^2\left\{\hat{W}_p - \frac{\Gamma\cos\theta}{\varepsilon_s\pi^2p^2(1+\lambda^2/12)}(1+(-1)^{p+1})\hat{U}\right\}^2. \end{aligned} \tag{29}$$

It is interesting to note that Eq. (28) is not a function of Γ or θ. Hence the only fundamental cable parameters that affect the direct out-of-plane response are ε_s and ξ_{yp}. Eq. (29) is a function of Γ and θ through κ_p as well as the term in $\hat{U}$, although for even p both these terms vanish and the equations for modes y_p and z_p are virtually identical.

The stability boundary for nonlinear modal coupling from mode z_p to y_p, Eq. (27), in non-dimensional form becomes

$$3(\hat{Z}_{pa}p\pi)^4 - 128\varepsilon_s\mu(\hat{Z}_{pa}p\pi)^2 + 1024\varepsilon_s^2(\mu^2 + \xi_{yp}^2) = 0. \tag{30}$$

This is not explicitly a function of Γ or θ , although if p is odd $\hat{Z}_{pa}$ is affected by these parameters as described above.

Solving Eq. (30) for $\hat{Z}_{pa}^2$, the y_p stability boundary occurs when

$$\hat{Z}_{pa}^2 = \frac{32\varepsilon_s\mu}{3\pi^2p^2}\left\{2 \pm \sqrt{1 - 3\left(\frac{\xi_{yp}}{\mu}\right)^2}\right\}. \tag{31}$$

This gives real solutions for $\mu > \xi_{yp}\sqrt{3}$. Below this frequency of excitation, mode y_p is always stable about the zero amplitude solution. Above this frequency, there are two stability boundaries. Mode y_p is unstable between these boundaries but stable for lower or higher amplitude motion in mode z_p (assuming no response in any other mode).

Substituting $\hat{Z}_{pa}^2$ from Eq. (31) into Eq. (29) gives the stability boundary in terms of the excitation frequency (μ) and amplitude (in braces on the right hand side of Eq. (29), where $\hat{W}_p$ and $\hat{U}$ have a fixed relationship—see Section 2.8).

The stability boundary for parametric excitation of mode y_q, Eq. (25), in non-dimensional form becomes

$$(\hat{Z}_{pa}p\pi)^4 - 32\varepsilon_s\mu(\hat{Z}_{pa}p\pi)^2 + 256\varepsilon_s^2(\mu^2 + \xi_{yq}^2) = \frac{16}{(1+\lambda^2/12)^2}\hat{U}^2. \tag{32}$$

This applies for even p, for which mode y_q exists with half the natural frequency of mode z_p.

Eq. (32) is a function of ε_s, but it is only a weak function of Γ and θ through λ^2 in the denominator of the right hand side. For taut cables, for which the original differential equations (Eqs. (2 and 3)) are valid, $\lambda^2/12 \ll 1$.

For parametric excitation of mode z_q, there is an identical stability boundary except ξ_{yq} is replaced by ξ_{zq} and μ by $(\mu-\kappa_q)$. Thus, for odd q, Γ and θ detune the stability boundary of mode z_q in comparison with mode y_q.

Solving Eq. (29) simultaneously with Eq. (32) (or the equivalent stability boundary for mode z_q) gives the stability boundary for parametric excitation in terms of the excitation frequency and amplitude. In this case the term in $\hat{U}$ in Eq. (29) is zero since p is even.

2.8. Excitation

A common use of inclined cables is in structures such as cable-stayed bridges and guyed masts. The cable end motions are then predominantly vertical at the lower anchorage and/or horizontal at the upper anchorage, so only these components are considered hereafter. A horizontal out-of-plane end motion does not include a component axial to the cable, so it cannot induce parametric excitation. Therefore, at the upper anchorage, only horizontal motion in the plane of the cable is considered. The end conditions used here are therefore

$$u_a = d_a \cos\theta, \quad v_a = 0, \quad w_a = -d_a \sin\theta,$$

$$u_b = d_b \sin\theta, \quad v_b = 0, \quad w_b = d_b \cos\theta, \tag{33}$$

where d_a is the horizontal in-plane displacement of the top anchorage and d_b the vertical displacement of the lower anchorage.

As stated in Section 2.1, it is assumed here that the rest of the structure to which the cable is attached is not affected by the dynamics of the cable. On cable-stayed structures, strictly there are dynamic interactions of the cable with the rest of the structure [14,19–23,33,34]. However, considering the global behaviour of the structure, since the mass of the other components (e.g. bridge deck and tower) are often much greater than the mass of the cables, the local cable vibrations are often ignored, which gives a reasonable representation of the global dynamics (see e.g. [35]). On this basis, neglecting any influence of the cable vibrations on the global structural vibrations, near resonance of a global mode of the structure the displacements of the cable ends are here taken as sinusoidal motions directly coupled to each other through the global mode shape, with the ratio ϕ (Fig. 2).

Hence the non-dimensional input amplitudes are given by

$$\begin{aligned} \hat{U} &= \hat{\Delta}(\sin\theta - \phi\cos\theta), \\ \hat{V}_n &= 0, \\ \hat{W}_n &= \hat{\Delta}((-1)^{n+1}\cos\theta - \phi\sin\theta), \end{aligned} \tag{34}$$

where $\hat{\Delta} = \Delta/L$ is the non-dimensional amplitude of vertical motion at the lower anchorage.

2.9. Typical results and significance of turning points

Fig. 3 shows a three-dimensional 'waterfall' plot of the steady-state direct response in mode z_2 (assuming no response in any other modes) from Eq. (29), for vertical excitation of the lower anchorage (and no motion of the upper anchorage) at a series of excitation frequencies close to its natural frequency. The parameters used are as for the experimental model in

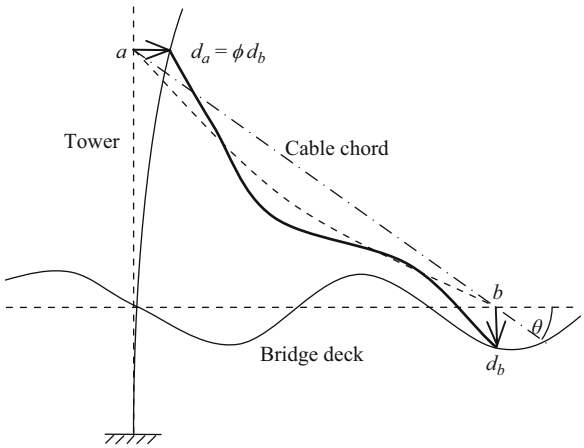

Fig. 2. Indicative dynamic displacements of a cable-stayed bridge in a global structural mode. Elevation view showing bridge deck, tower and one cable (other cables omitted for clarity). Dashed lines: static shape. Solid lines: dynamic shape.

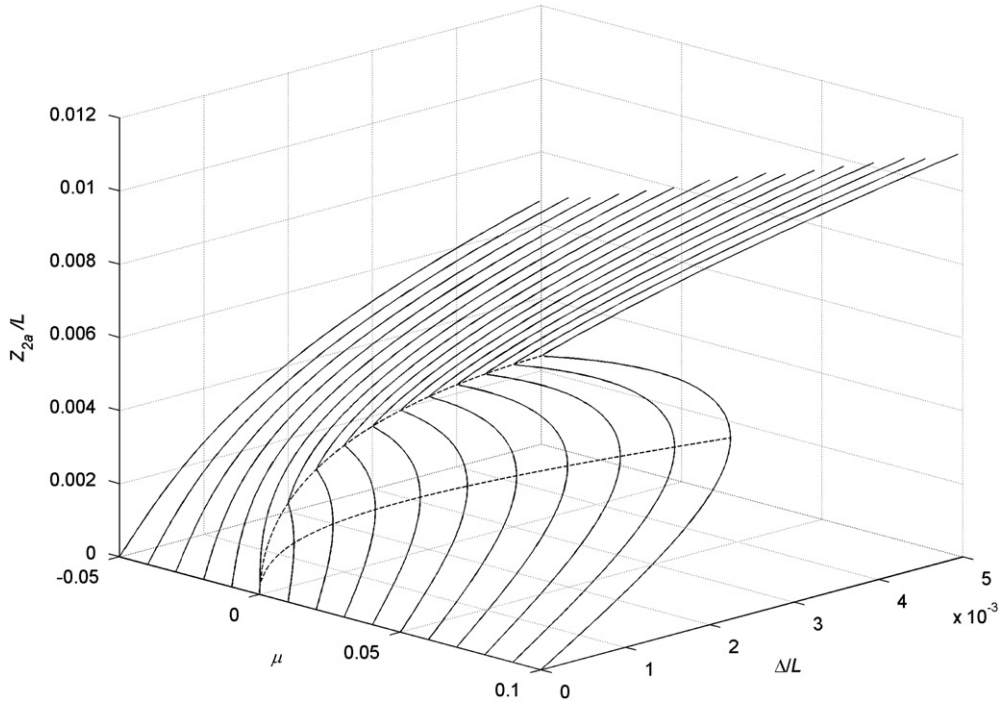

Fig. 3. Three-dimensional 'waterfall' plot of steady-state response amplitudes in second in-plane mode. Dotted lines show the loci of the turning points demarking the fold.

Table 1
Experimental cable parameters.

Basic cable data	
Length, L	5.40 m
Inclination angle, θ	22.6°
Total mass per unit length[a], ρA	0.231 kgm^{-1}
Diameter	0.79 mm
Young's modulus, E	214×10^{9} Nm^{-2}
Static tension along chord, $\sigma_s A$	286 N
Non-dimensional parameters	
$\varepsilon_s=\sigma_s/E$	2.73×10^{-3}
$\Gamma=\rho g L/\sigma_s$	0.0429
Irvine's parameter, $\lambda^2=\Gamma^2\cos^2\theta/\varepsilon_s$	0.57
Measured damping ratio[b]	0.02%

[a] Including added masses.
[b] Found to be similar in all modes.

Section 3 and Table 1. It is clear that for excitation frequencies below the natural frequency ($\mu<0$) the response amplitude increases monotonically with the input amplitude, but for excitation frequencies above the natural frequency there is a fold in the response amplitude. In general, from Eq. (29), the turning points (loci shown by dotted lines in Fig. 3) occur at

$$\hat{Z}_{pa}^2=\frac{32\varepsilon_s(\mu-\kappa_p)}{9\pi^2p^2}\left\{2\pm\sqrt{1-3\left(\frac{\xi_{zp}}{\mu-\kappa_p}\right)^2}\right\}. \tag{35}$$

Real solutions only exist for $\mu-\kappa_p>\xi_{zp}\sqrt{3}$, hence the fold only exists for excitation frequencies that satisfy this criterion.

The direct response amplitudes of mode z_2 are re-plotted for four representative excitation detuning values (μ) in Fig. 4, which also shows the stability boundaries of modes z_1, y_1 and y_2, from Eqs. (30) and (32) (and the equivalent for mode z_1). Following the curve from the origin, each of these modes is initially stable and its stability changes passing each marked point. (Strictly, when any one of these modes is unstable the calculated Z_{2a} response and any other instability points are not valid, since they were based on the assumption of a non-zero response only in the directly excited mode.)

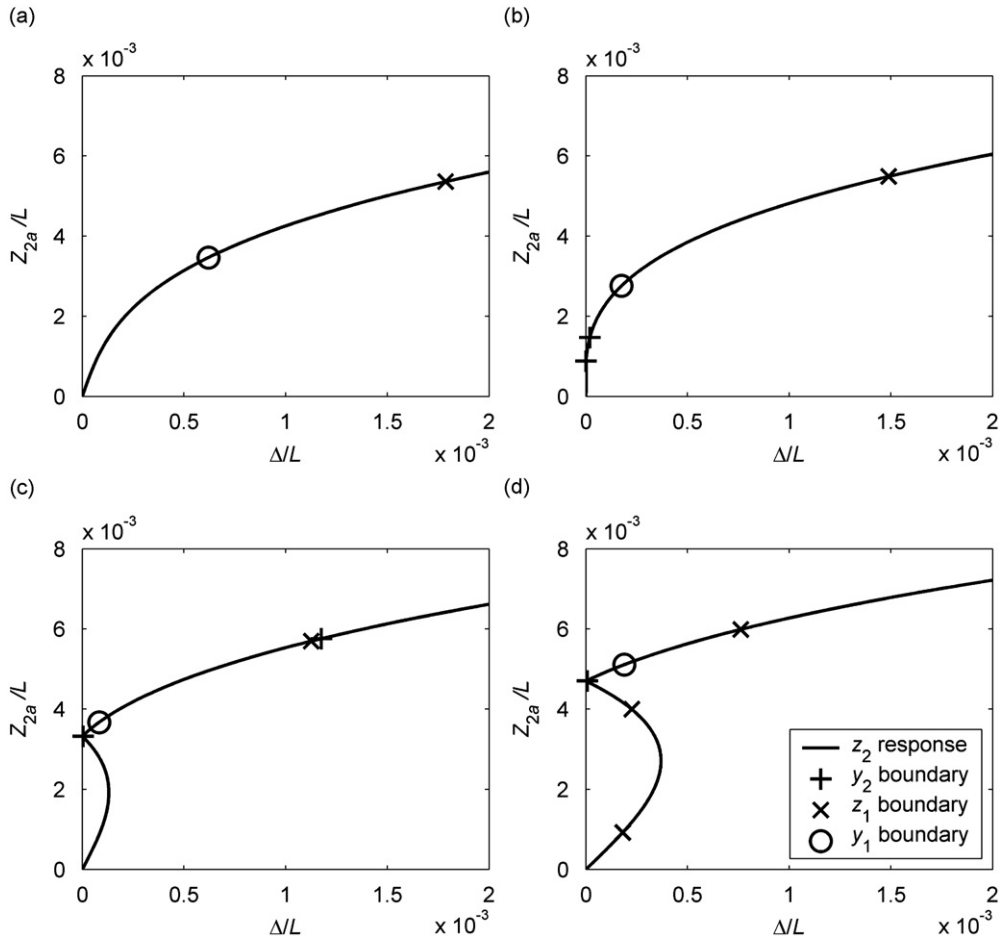

Fig. 4. Steady-state response amplitudes in second in-plane mode, showing stability boundaries of other modes. Following the curve from the origin, each mode is initially stable and the stability changes passing each point. (a) $\mu=-0.010$, (b) $\mu=0.001$, (c) $\mu=0.015$, (d) $\mu=0.030$.

The importance of the turning points can be seen in Fig. 4(c). The y_1 and y_2 instability points exist at very low values of Δ/L, but on the upper branch of the z_2 response. Starting from the origin, for increasing excitation amplitudes the solution will follow the lower branch. Instability of mode y_1 or y_2 does not occur until the solution jumps onto the upper branch at the lower (in terms of $\hat{Z}_{pa}$) turning point. Hence, for practical initial conditions, this turning point, rather than the theoretical stability boundary, determines the minimum excitation amplitude for the instability to occur.

The excitation amplitude at the turning point can be found, in relation to the excitation frequency, by substituting Eq. (35) (using the negative square root) back into Eq. (29).

3. Laboratory experiments

A series of laboratory experiments were conducted on an inclined cable to validate the analysis. The cable was made from piano wire and was 5.40 m long (Fig. 5), with suitable static tension applied and lumped masses added so that the non-dimensional cable parameters matched typical values for a 200 m long bridge cable. The cable parameters are given in Table 1 and its theoretical and experimental natural frequencies in Table 2. The cable model was similar to a previous 1.98 m long model used [25], except for its larger scale and the use of a hydraulic actuator for excitation of the lower anchorage, enabling better control of the input motion, especially for higher frequencies and lower amplitudes. Inputs up to at least 15 Hz (>4 times the cable fundamental natural frequency) and down to approximately 0.1 mm amplitude ($2\times10^{-5}L$) could be accurately controlled.

The upper anchorage was fixed and the lower anchorage was constrained to move only vertically by a simply supported beam, which also carried the horizontal component of the cable tension. The vertical displacement of the anchorage was measured by a linear variable differential transformer (LVDT), which was also used for feedback control of the hydraulic actuator. The tension in the cable was measured at both ends with load cells, while the motion of the central and lower quarter points of the cable were tracked in both planes with a video displacement measurement system [36].

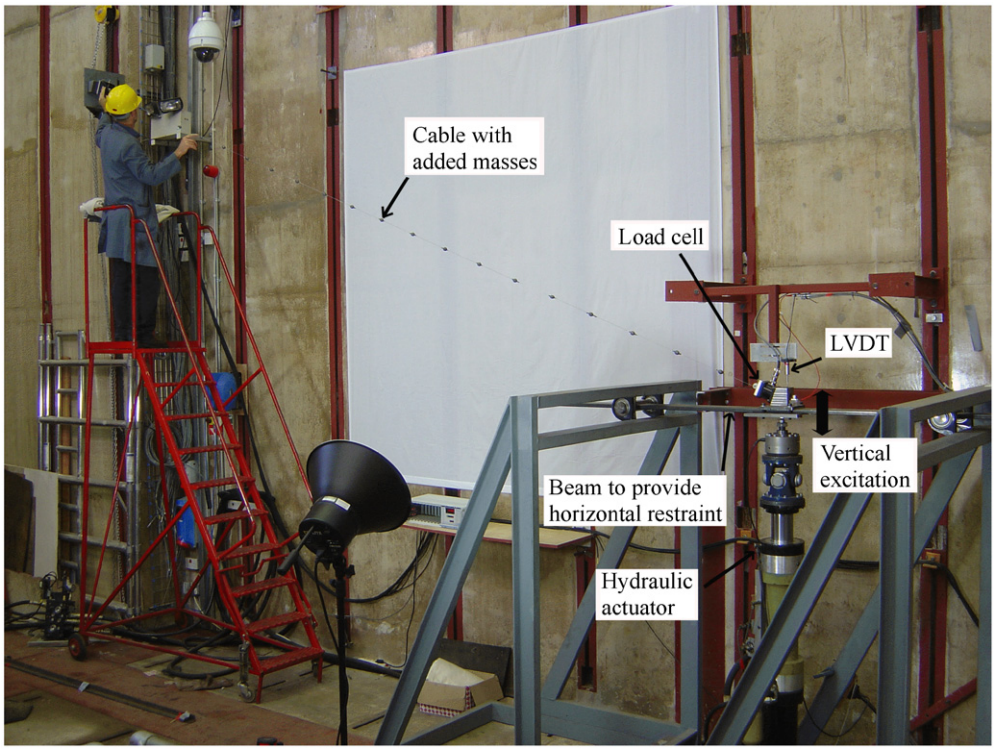

Fig. 5. Photograph of experimental rig.

Table 2
Cable natural frequencies.

Mode no. (n)	Out-of-plane (y_n)			In-plane (z_n)		
	Theoretical (Hz)	Measured (Hz)	Error (%)	Theoretical (Hz)	Measured (Hz)	Error (%)
1	3.255	3.254	−0.03	3.331	3.330	−0.03
2	6.509	6.494	−0.23	6.509	6.496	−0.20
3	9.764	9.726	−0.39	9.767	9.725	−0.43
4	13.019	12.907	−0.86	13.019	12.897	−0.94

Sinusoidal input motions were applied at a series of frequencies close to the first four natural frequencies of the cable. Before each test any cable vibrations were manually stopped then allowed to decay away further so the initial conditions were as close as possible to at rest. The input amplitude was ramped up over 20 s to minimise transient effects. At each frequency, a series of tests was carried out with amplitude increments of 0.2 mm ($3.7\times10^{-5}L$) until an instability of any mode other than the directly excited mode occurred. Tests typically ran for 330 s each (over 1000 times the fundamental vibration period) to give sufficient time for instabilities to develop and often for the steady-state response to be reached. In the following figures the experimental points show the minimum input amplitude for which an instability was found. An input with an amplitude 0.2 mm ($3.7\times10^{-5}L$) lower did not cause the instability to occur within the test period. The steady-state amplitudes of the directly excited mode are also presented for these tests just below the stability boundaries.

4. Theoretical and experimental stability boundaries

The stability boundaries are considered, both theoretically and experimentally, for excitation around each of the first four natural frequencies of the cable. These instances exhibit all the characteristics of the modal instabilities that occur in the general case. The behaviour for excitation around the third and fourth natural frequencies is typical for inputs close to higher odd and even natural frequencies respectively. Excitation around the first and second natural frequencies exhibit different features due to the significant detuning of the first in-plane mode (z_1) relative to the commensurate series of the other modes, because of the cable sag.

Only the steady-state response of the directly excited mode and the first loss of stability of any other modes are considered, since the theory presented does not describe the behaviour thereafter. However, this defines the boundaries above which more damaging vibrations could occur.

The theoretical results use the parameter values for the cable in Table 1. The measured natural frequencies of the first mode in each plane matched extremely well with the theoretical values (Table 2). For higher modes the differences increased slightly, up to 1%, believed to be due to the use of the added lumped masses on the physical model (Section 3). The measured damping ratio of 0.02% (found to be similar in all modes) was used in the calculations. This is a very low damping ratio, but comparable values have been found on site for the structural damping of cable-stayed bridge cables with no added dampers [37]. Since the damping is so low, steady-state amplitudes in the directly excited mode are generally governed by nonlinearity rather than damping.

4.1. Excitation around third natural frequency

Excitation around the third natural frequency (p=3) is the simplest case so is considered first. From Eq. (4), for the experimental cable parameters the theoretical detuning of the in and out-of-plane natural frequencies, κ_3, is only 2.9×10^{-4}, while the measured detuning is -1.0×10^{-4}. Hence the modes are almost perfectly tuned with each other. Mode z_3 is excited directly and since p is odd, there is no parametric excitation. The only potential instability is therefore of mode y_3, due to nonlinear modal coupling. The stability boundary is plotted in Fig. 6(a), the unstable region being in the upper right sector. However, the lower stability boundary (close to the horizontal axis), is on the upper branch of the z_3 solution. Hence with small initial conditions, in practice mode y_3 becomes unstable at the lower turning point of z_3, as described in Section 2.9. The locus of the turning point is also plotted in Fig. 6(a), which matches very well with the experimentally identified instability points of mode y_3. (In Fig. 6 onwards, lines indicate theoretical results whereas discrete symbols show experimental results. The turning point plotted is the lower one (in terms of $\hat{Z}_{pa}$). The upper turning point is of no practical significance so is not plotted.)

The instability only occurs above the natural frequency due to the stiffening behaviour of the cable. The amplitude of the directly excited mode is larger for positive detuning than for negative, so it is able to reach the critical amplitude for the out-of-plane mode to become unstable. Similarly the fold only occurs for positive detuning due to the stiffening behaviour.

The steady-state amplitudes of mode z_3 for excitation just below the turning point (and just below the theoretical instability boundary) are shown in Fig. 6(b). The experimental results show reasonable agreement with the theory. A slightly higher input amplitude causes a jump in the z_3 response amplitude onto the higher branch, which is then in the instability region for mode y_3. It is believed likely that the experimental points are below the locus of the theoretical turning point in Fig. 6(b) since the points plotted are the maximum steady-state amplitudes measured below the turning point, where the gradient of the z_3 amplitude, Z_{3a}, with respect to the input amplitude, Δ, is high (c.f. Fig. 4(c) and (d)). Hence for Δ just below the turning point, Z_{3a} could be significantly below it.

Excitation around higher odd natural frequencies should exhibit virtually the same behaviour as for p=3, since parametric excitation does not occur and the natural frequencies of the modes in the two planes are almost precisely tuned to each other.

4.2. Excitation around fourth natural frequency

For excitation around the fourth natural frequency (p=4), the same features occur as for p=3, although there is theoretically perfect tuning between modes y_4 and z_4. In addition, parametric excitation of the second in or out-of-plane

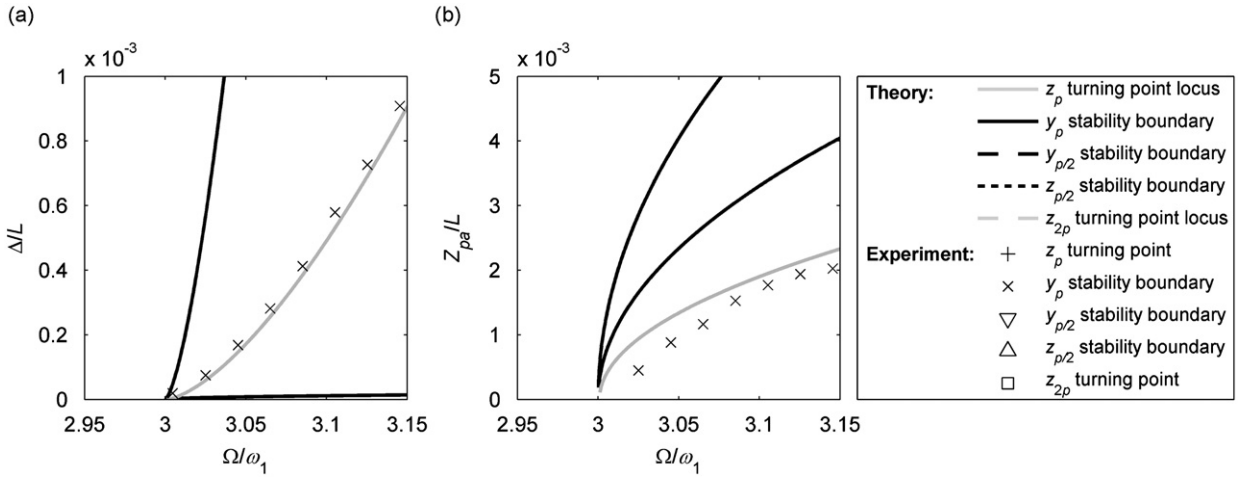

Fig. 6. Stability boundary and turning point for excitation around third natural frequency (p=3). (a) Excitation frequency and amplitude on stability boundary and at turning point. (b) Steady-state amplitude of mode z_3. Legend applies to Figs. 6–8 and 10.

modes could occur. Since $\kappa_2=0$ and the damping of the two second modes is taken to be the same, the stability boundaries of these two modes, due to parametric excitation, are theoretically identical. They are plotted in Fig. 7(a), along with the stability boundary for mode y_4 and the locus of the turning point of mode z_4 (directly excited).

Similarly to the case for nonlinear modal coupling, the instability region for parametric excitation is in the top right sector and the lower boundary is on the upper branch of the solution for the directly excited mode. Therefore the input amplitudes at which the instabilities occur in practice is given by the locus of the turning point of the directly excited mode. Theoretically, the z_4 response then jumps to an amplitude at which modes y_2, z_2 and y_4 are all unstable. Experimentally it was found that mode y_4 normally grew first and that the input amplitude at which this occurred agreed very well with the theoretical turning point.

The steady-state amplitudes of mode z_4 just below the turning point (and just below the theoretical instability boundaries) are plotted in Fig. 7(b). The experimental points follow a similar trend to the locus of the theoretical turning point. As for excitation with $p=3$ (Fig. 6), the measured steady-state amplitudes in Fig. 7(b) are below the theoretical curve, whereas the input amplitudes in Fig. 7(a) are generally above the curve with smaller errors.

Excitation around higher even natural frequencies should exhibit virtually the same behaviour as for $p=4$, since parametric excitation can occur and the theoretical natural frequencies of the four relevant modes have the same ratios.

4.3. Excitation around second natural frequency

For excitation around the second natural frequency ($p=2$) the situation is complicated further. Similarly to before, mode z_2 is excited directly, and mode y_2, theoretically with the same natural frequency, can become unstable due to nonlinear modal coupling. Modes y_1 and z_1 can be excited parametrically, but the natural frequency of z_1 is significantly detuned from y_1 (and half the natural frequency of y_2 and z_2) by the cable sag.

Fig. 8 shows the stability boundaries and the locus of the z_2 turning point. The stability boundaries for modes y_1 and y_2 are equivalent to those for modes y_2 and y_4 for excitation with $p=4$ (Fig. 7). In the excitation frequency range $2.006\omega_1-2.040\omega_1$ in practice the amplitude required for instability is governed by the turning point, above which both modes are unstable. Experimentally mode y_2 was found to grow first, for inputs in very good agreement with the locus of the theoretical turning point.

For input frequencies below $2\omega_1$ (theoretically $2.00069\omega_1$—see Section 2.7) mode y_2 is always stable, and below the same frequency (since $\kappa_2=0$) there is no turning point in the z_2 response (see Section 2.9). Hence below this frequency, the relevant modal instability is parametric excitation of mode y_1. This instability was found experimentally, in very good agreement with the theoretical stability boundary.

The stability boundary for parametric excitation of mode z_1 has a minimum at $2.047\omega_1$, i.e. two times its natural frequency ($\kappa_1=0.0236$). Above an excitation frequency of $2.040\omega_1$ the boundary exists on the lower branch of the z_2 response. Therefore it is on the theoretical stability boundary itself, rather than at the turning point (which occurs at larger input amplitudes), at which the instability occurs in practice. This was confirmed experimentally, again in very good agreement with the theory, as seen in Fig. 8(a). Strictly there are two other solutions for the z_1 stability boundary but they occur on the unstable and upper branches of the z_2 solution, and they are not of practical relevance, so they are omitted from Fig. 8(a) for clarity.

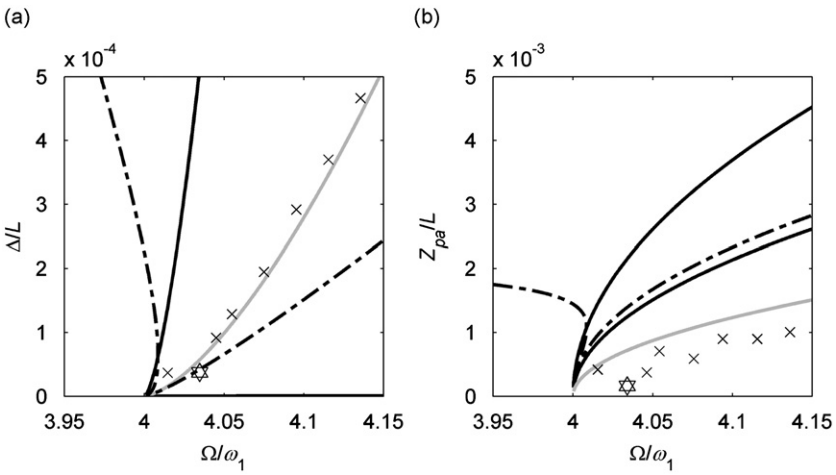

Fig. 7. Stability boundaries and turning point for excitation around fourth natural frequency ($p=4$). (a) Excitation frequency and amplitude on stability boundaries and at turning point. (b) Steady-state amplitude of mode z_4. Legend as for Fig. 6 ($y_{p/2}$ and $z_{p/2}$ theoretical stability boundaries are superimposed and appear as a chain dotted line).

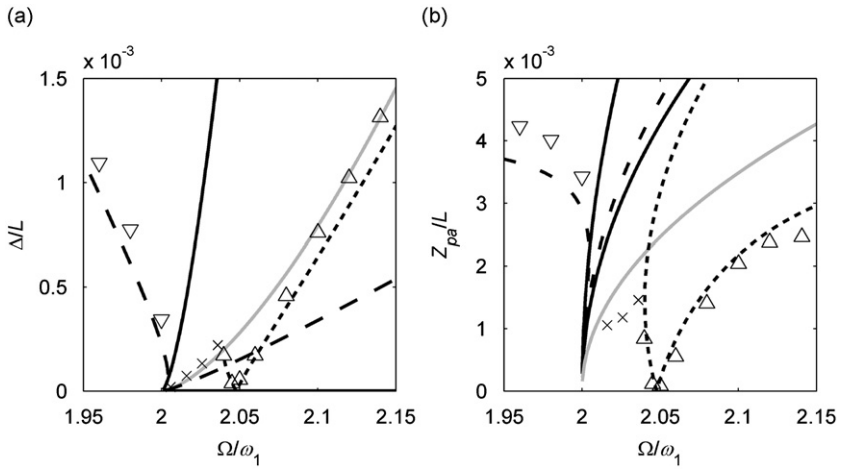

Fig. 8. Stability boundaries and turning point for excitation around second natural frequency (p=2). (a) Excitation frequency and amplitude on stability boundaries and at turning point. (b) Steady-state amplitude of mode z_2. Legend as for Fig. 6.

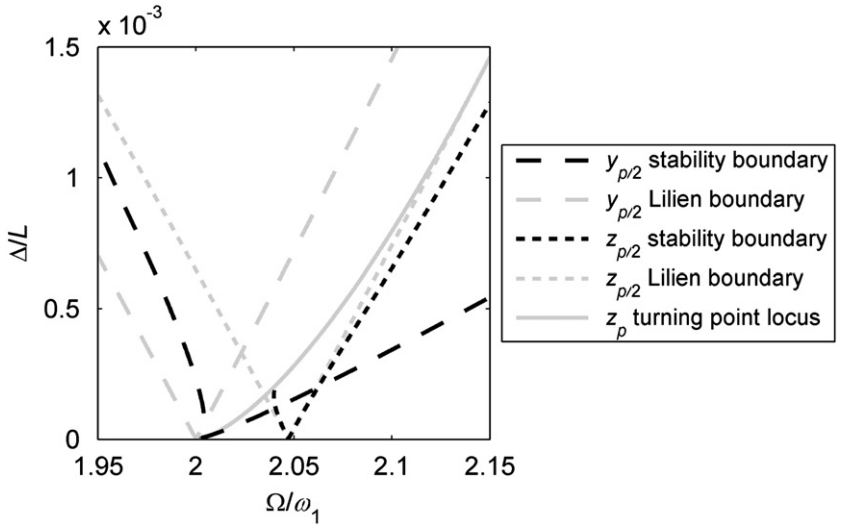

Fig. 9. Comparison between stability boundaries for parametric excitation from Lilien and Pinto da Costa [5] and current analysis (around second natural frequency, p=2).

The steady-state amplitudes of mode z_2 for excitation just below the stability boundaries and the turning point are shown in Fig. 8(b). The experimental results show reasonable agreement with the theory for the boundaries for all three types of instability.

The stability boundaries for parametric excitation are compared between the current analysis and those from Lilien and Pinto da Costa [5] (Eq. (1)) in Fig. 9. The difference is that the current analysis includes the effect of the directly excited mode, whereas Lilien and Pinto da Costa considered the parametrically excited mode alone. There is a marked difference for the mode y_1 stability boundary, which is experimentally confirmed to be accurate in the current analysis in Fig. 8(a). Relative to the solution from Lilien and Pinto da Costa, for the actual stability boundary the necessary input amplitude is generally increased for excitation frequencies below the natural frequency and decreased above it. This can be explained by the fact that the directly excited response increases the mean tension, hence it effectively increases the natural frequency, moving the stability boundary to the right. The magnitude of this shift is dependent on the response amplitude, giving rise to the new stability boundary shown. The minimum input amplitude for parametric excitation is not affected significantly, since the directly excited response is then small and the boundary is then governed by the damping ratio rather than the cable nonlinearity. But it is noteworthy that for excitation frequencies above the natural frequency the cable is considerably more susceptible to parametric excitation of mode y_1 than previously thought.

For parametric excitation of mode z_1, the difference between the actual stability boundary and that given by Lilien and Pinto da Costa [5] (substituting ω_{z1} for ω_1 in Eq. (1)) is less pronounced than for mode y_1 (Fig. 9). This is because of the

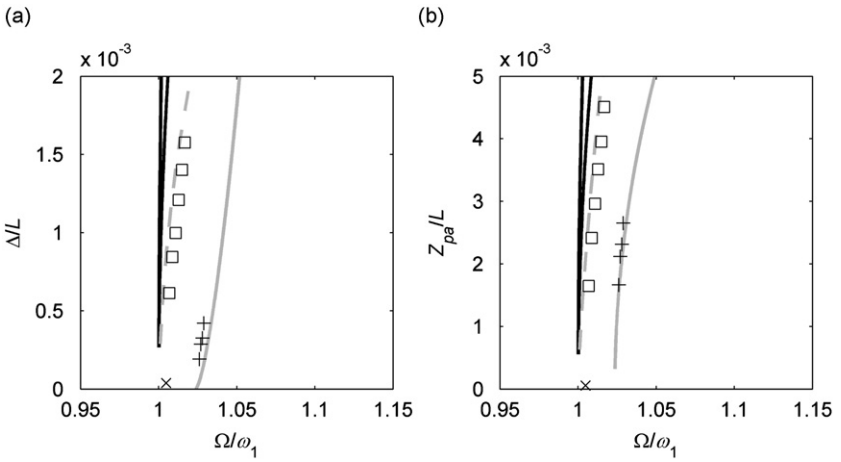

Fig. 10. Stability boundary and turning points for excitation around first natural frequency (p=1). (a) Excitation frequency and amplitude on stability boundary and at turning points. (b) Steady-state amplitude of mode z_1. Legend as for Fig. 6.

detuning of mode z_1 from the commensurate series of the others. Hence in the frequency range for parametric excitation of mode z_1, the directly excited mode (z_2) is excited further from its natural frequency than the equivalent mode in the y plane, so its response amplitude is smaller, so it has less effect on the behaviour of mode z_1. However, for taut or steeply inclined cables, the detuning of mode z_1 from the others is smaller, so it is more affected by the response in mode z_2. In any case the parametric excitation of all other modes is greatly affected by the directly excited mode, so the standard analysis [5,8], based on a single mode analysis, is inadequate.

4.4. Excitation around first natural frequency

Finally, excitation around the first natural frequency (p=1) is considered. Similarly to p=3 (Section 4.1), parametric excitation does not occur and the only potential instability is through modal coupling with the equivalent out-of-plane mode (y_1). However, since mode z_1 is significantly detuned from y_1 (κ_1=0.0236), much larger input amplitudes are required for z_1 to reach the critical amplitude for y_1 to go unstable (still defined by Eq. (31)). For the same reason, the turning point of mode z_1 occurs for higher detuning of the excitation frequency from ω_1.

Fig. 10(a) shows the locus of the turning point for mode z_1 which exists above an excitation frequency of $1.024\omega_1$ (see Section 2.9). It is very well matched by the experimental data. In addition, in these tests the steady-state amplitude of mode z_1 just below the turning point matched the theoretical values very well, as shown in Fig. 10(b).

The theoretical stability boundary for mode y_1 is also shown in Fig. 10, but it demarks an extremely narrow instability tongue at an excitation frequency of $1.00\omega_1$. In one test, at an excitation frequency of $1.002\omega_1$, instability of mode y_1 occurred. The input amplitude was somewhat below the minimum of the theoretical stability curve, but it is sensitive to the damping ratio, which by its nature contains some uncertainty (other stability boundaries are governed more by the nonlinearities than the damping ratio, so they would be less sensitive to such an error).

No instability boundary or turning point was found for excitation at frequencies below ω_1. However, while searching for the y_1 instability boundary in experiments for excitation frequencies just above ω_1, unexpected large responses of mode z_2 at twice the excitation frequency (i.e. near its natural frequency) were found. Other super-harmonic responses of cables have previously been considered [20,21,38,39], but the explanation of the observed behaviour required a refinement of the current analysis, described in the following section.

5. Response at twice excitation frequency

It was previously assumed that it was adequate to consider the response in each mode only to occur close to its natural frequency (Eq. (9)). However, a better representation of the response is given by including a non-resonant component of response at the excitation frequency. Hence z_n is expressed as

$$z_n = z_{nc}\cos(\omega_n\tau) + z_{ns}\sin(\omega_n\tau) + z_{np}\cos(\omega_p\tau). \tag{36}$$

(Note $\omega_p\tau = \Omega t$.) It can easily be shown that the sine component of the non-resonant response is negligible. For excitation close to resonance (n=p), z_{pp}=0, since the response is already covered by the z_{nc} and z_{ns} terms.

The parametric excitation term in Eq. (3), $2\eta_n(u_b-u_a)z_n$, then leads to an additional term on the right hand side of Eq. (15) equal to

$$-\frac{\varepsilon}{\omega_n}\delta_{n,2p}\frac{\eta_n}{2m}Uz_{npa}. \tag{37}$$

Hence the directly excited non-resonant component of mode $n=2p$, z_{2ppa}, leads to excitation of the resonant component of the same mode. Strictly other nonlinear terms also arise. However, for low amplitude response of mode $2p$ the additional nonlinear terms are small relative to the existing nonlinear terms involving the directly excited resonant response of mode z_p.

It should be noted that the additional term (37) is an excitation term, present even at very low amplitudes and it cannot be fitted into the form of Eq. (20). Hence the resonant response of mode z_{2p} is not a matter of stability but of magnitude.

Assuming the non-resonant response of any mode to be linear, since it is small, its steady-state amplitude is given by

$$\begin{aligned} z_{npa} &= \frac{(\zeta_n W_n-\alpha_n U)}{m}\frac{\Omega^2}{\omega_{zn}^2-\Omega^2} \\ &\approx \frac{(\zeta_n W_n-\alpha_n U)}{m}\frac{p^2}{n^2-p^2}. \end{aligned} \tag{38}$$

The amplitude of the non-resonant response of mode z_{2p} is then

$$\begin{aligned} z_{2ppa} &= \frac{\zeta_{2p}W_{2p}}{3m} \\ &= \frac{W_{2p}}{3p\pi}. \end{aligned} \tag{39}$$

Ignoring the additional nonlinear terms mentioned above and assuming that the response of mode z_p is unaffected by the response of mode z_{2p} (reasonable if it is small), the steady-state resonant response of mode z_{2p} is given by

$$\begin{aligned} &9(\hat{Z}_{2pa}2p\pi)^6-192\varepsilon_s\left[\mu-\frac{(\hat{Z}_{pa}p\pi)^2}{16\varepsilon_s}\right](\hat{Z}_{2pa}2p\pi)^4 \\ &+1024\varepsilon_s^2\left\{\left[\mu-\frac{(\hat{Z}_{pa}p\pi)^2}{16\varepsilon_s}\right]^2+\xi_{z2p}^2\right\}(\hat{Z}_{2pa}2p\pi)^2=\frac{256}{9}\hat{W}_{2p}^2\hat{U}^2. \end{aligned} \tag{40}$$

This is similar to the equation for the steady-state amplitude of mode z_p (Eq. (29)), except for the different excitation term (squared) on the right hand side of the equation, $\kappa_{2p}=0$, since $2p$ is even, and there are correction terms to the detuning, μ, to account for the directly excited response in mode z_p.

For in-plane excitation of the form described in Section 2.8, considering the input amplitudes, Eqs. (34), the excitation term of mode z_{2p} is proportional to $\hat{\Delta}^2$. It arises from the combination of the transverse component of the support motion, W_{2p}, exciting a non-resonant response of the mode and the axial component of the support motion, U, causing a tension variation oscillating in phase with the non-resonant modal response. This combination provides the quadratic forcing term which drives the resonant response in mode z_{2p}, at twice the excitation frequency. In common with the effect of the directly excited mode z_p modifying the parametric excitation of mode y_q or z_q (where $q=p/2$), this phenomenon is due to the support motion having components both axial and transverse to the cable. Although combined parametric and external excitation has been studied theoretically [10,11,40–42] and it is inherent in other treatments of the inclined cable system considered here [7,12,13,15–18,39], this particular excitation mechanism has not previously been identified. This new mechanism is not dependent on modal interactions – it still occurs in a single-degree-of-freedom model (for mode z_{2p}) – although it is modified by the directly excited response in mode z_p, according to the terms in square brackets in Eq. (40).

Similarly to the steady-state response of mode z_p, there can be a fold in the resonant response of mode z_{2p}. The turning points are given by an expression similar to Eq. (35). However, it is a function of the amplitude of the response in mode z_p, which is itself a nonlinear function of the input amplitude. It is therefore not possible to derive an explicit equation relating the support amplitude and frequency at the turning points. The position of the fold has therefore been calculated numerically. It is the jump in the z_{2p} resonant response from its lower turning point that was found experimentally in the tests with $p=1$ (Section 4.4). Fig. 10 shows the theoretical and experimental turning points, which are in very good agreement.

The assumptions above are only valid for small amplitude response of mode z_{2p}. They therefore give a reasonable estimate of the behaviour before the jump and the input amplitude at which the jump occurs. However, the analysis is unlikely to be accurate thereafter, since the nonlinear terms involving mode z_{2p} are no longer negligible. In Fig. 10, the y_1 stability boundary is then likely to be modified by the z_2 response.

To indicate the importance of the response at twice the excitation frequency for input frequencies just above ω_1, the various components of the cable response are shown in Fig. 11 for an excitation frequency of $1.008\,\omega_1$ ($p=1$). The theoretical directly excited response amplitude in mode z_1 ($\hat{Z}_{pa}$ from Eq. 29) is shown as a solid line. For low excitation amplitudes it is much larger than both the non-resonant and resonant components of response of mode z_2 (z_{2ppa}/L from

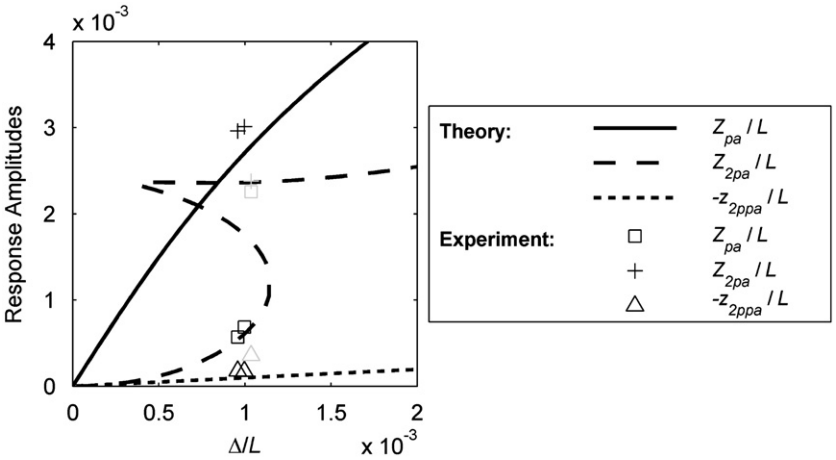

Fig. 11. Steady-state response amplitudes of different components of cable motion for excitation frequency $1.008\omega_1$ ($p=1$). Black symbols: experimental amplitudes before jump in z_{2p} response. Grey symbols: experimental amplitudes after jump in z_{2p} response.

Eq. (39) and $\hat{Z}_{2pa}$ from Eq. (40), respectively). For increasing excitation amplitude the non-resonant response of mode z_2 remains small, increasing linearly as assumed. However, the resonant response of mode z_2, at twice the excitation frequency, increases much more rapidly, since it is driven by the excitation amplitude squared. For an excitation amplitude of $\hat{\Delta} = 1 \times 10^{-3}$ it has theoretically reached a response amplitude of 23% of the directly excited response of mode z_1. From filtering of the measured responses at the cable mid and lower quarter points, Fig. 11 shows the experimental amplitudes of the different response components at two excitation amplitudes just below 1×10^{-3}. There is very good agreement with the theory for the amplitude of all three response components, giving confidence in the analysis. For a very small increment in the excitation amplitude, experimentally there was then a jump in the resonant response amplitude of mode z_2 of more than a factor of three. Although there was a slight discrepancy with the theoretical excitation amplitude for the jump (but note from Fig. 10 it is very sensitive to the detuning of the excitation and natural frequencies), the behaviour was otherwise as expected. The experimental points above the jump are shown in Fig. 11 in grey, indicating that good agreement with the theory is no longer expected since the assumption of small response in mode z_2 is no longer valid. The experimental resonant response of mode z_2 is, in this case, nevertheless still very close to the theoretical response, although the other components of response show larger discrepancies. The resonant response of mode z_2 is very similar in amplitude to the directly excited response in mode z_1, showing the importance of the response at twice the excitation frequency in these circumstances. The behaviour at other excitation frequencies in this vicinity is very similar.

After the jump, experimentally mode y_2 was found to be unstable. This is believed to be due to nonlinear coupling with mode z_2, similar to the coupling from mode z_p to y_p (Section 2.6). However, the behaviour would be modified by the response in both modes z_1 and z_2, the analysis of which is beyond the scope of this paper.

For taut cables the response of mode z_{2p} is only significant for $p=1$. For larger p, the response of mode z_{2p} is smaller and the stability boundaries for the other modes are lower than its theoretical turning point. It is important for $p=1$ since the directly exited response in mode z_1 is detuned from $\mu=0$, so other effects are more significant.

6. Conclusions

Generalised stability boundaries of modal vibrations have been presented for a cable subjected to harmonic support excitation near any natural frequency. The underlying cable model allows for cable inclination, small sag, cubic and quadratic geometric nonlinearities (from cable stretching and its interaction with the static sag respectively), multiple modes in both planes (with nonlinear coupling between them) and motion of cable ends in any direction. The results concentrate on the case of in-plane excitation – vertical at the lower anchorage or equivalently horizontal at the upper anchorage – which is the most significant condition for cables on cable-stayed bridges and guyed masts.

For inputs with components both normal to and along the cable, single mode analysis is not adequate. The response in the directly excited mode, mainly from the normal component, affects the stability boundaries of the other modes. In particular, for excitation above the natural frequency, the cable is unstable for lower amplitude inputs than previously believed.

Modal instabilities can occur from two mechanisms: (a) nonlinear modal coupling between modes in the two planes with the same natural frequencies, governed by the amplitude of the directly excited mode, or (b) parametric excitation, at half the excitation frequency, in either plane, due to the axial component of the end motion. Often in practice modal instability occurs when the directly excited response passes a turning point rather than on the theoretical stability boundary itself, which often occurs on the upper branch of the directly excited response.

Although the cable model initially includes all modes, normally the only important modes are the two at the excitation frequency and, for direct excitation of even modes, the two at half the excitation frequency.

Theoretical and experimental stability boundaries have been presented for a cable with typical non-dimensional parameter values for excitation around the first four natural frequencies. Excitation around the third and fourth natural frequencies gives behaviour typical of higher modes, with virtually perfect tuning between the modes. Excitation around the first and second natural frequencies are special cases due to the detuning of the first in-plane mode, caused by the cable sag.

For excitation around the first natural frequency, in addition, significant response of the second in-plane mode can occur, at two times the excitation frequency. This is another consequence of the combination of components of the excitation along and normal to the cable, providing combined parametric and external excitation. This is the first time this particular mechanism has been identified.

In all cases there is good agreement between the theoretical and experimental responses, validating the underlying equations of motion from Warnitchai et al. [26] for this application with taut inclined cables, and giving confidence in the theoretical expressions derived here. These expressions define the conditions under which instabilities or jumps in modal responses occur, which could lead to damaging large amplitude vibrations.

Acknowledgments

This work was supported by EPRSC, principally through Grant GR/T28270/01 and also through JHGM's Advanced Research Fellowship and support for AGB under Grant GR/S49780/01.

References

[1] A.H. Nayfeh, P.F. Pai, in: *Linear and Nonlinear Structural Mechanics*, Wiley, 2004.
[2] G. Rega, Nonlinear vibrations of suspended cables—part1: modeling and analysis, *Applied Mechanics Review* 57 (6) (2004) 443–478.
[3] G. Rega, Nonlinear vibrations of suspended cables—part II: deterministic phenomena, *Applied Mechanics Review* 57 (6) (2004) 479–514.
[4] R.A. Ibrahim, Nonlinear vibrations of suspended cables—part III: random excitation and interaction with fluid flow, *Applied Mechanics Review* 57 (6) (2004) 515–549.
[5] J.L. Lilien, A. Pinto da Costa, Vibration amplitudes caused by parametric excitation of cable-stayed structures, *Journal of Sound and Vibration* 174 (1) (1994) 69–90.
[6] G. Tagata, Harmonically forced, finite amplitude vibration of a string, *Journal of Sound and Vibration* 51 (4) (1977) 483–492.
[7] R. Uhrig, On kinetic response of cables of cable-stayed bridges due to combined parametric and forced excitation, *Journal of Sound and Vibration* 165 (1) (1993) 185–192.
[8] SETRA, Cable Stays; Recommendations of French interministerial commission on prestressing, Center des Techniques des Ouvraes d'Art, Bagneux Cedex, France, 2002.
[9] E.S. Caetano, Indirect excitation of stays on cable-stayed bridges, *Proceedings of the Fourth International Symposium on Cable Dynamics*, Montreal, 2001, pp.129–136.
[10] N.C. Perkins, Modal interactions in the non-linear response of elastic cables under parametric/external excitation, *International Journal of Non-linear Mechanics* 27 (2) (1992) 233–250.
[11] W. Zhang, Y. Tang, Global dynamics of the cable under combined parametrical and external excitations, *International Journal of Non-Linear Mechanics* 37 (2002) 505–526.
[12] A. Berlioz, C.-H. Lamarque, A non-linear model for the dynamics of an inclined cable, *Journal of Sound and Vibration* 279 (3-5) (2005) 619–639.
[13] C.T. Georgakis, C.A. Taylor, Nonlinear dynamics of cable stays—part 1: sinusoidal cable support excitation, *Journal of Sound and Vibration* 281 (2005) 537–564.
[14] C.T. Georgakis, C.A. Taylor, Nonlinear dynamics of cable stays—part 2: stochastic cable support excitation, *Journal of Sound and Vibration* 281 (2005) 565–591.
[15] L. Wang, Y. Zhao, Large amplitude motion mechanism and non-planar vibration character of stay cables subject to the support motions, *Journal of Sound and Vibration* 327 (1-2) (2009) 121–133.
[16] A. Pinto da Costa, J. Martins, F. Branco, J.L. Lilien, Oscillations of bridge stay cables induced by periodic motions of deck and/or towers, *ASCE Journal of Engineering Mechanics* 122 (1996) 613–622.
[17] Y. Cai, S.S. Chen, Dynamics of elastic cable under parametric and external resonances, *ASCE Journal of Engineering Mechanics* 120 (8) (1994) 1786–1802.
[18] S.A. Nayfeh, A.H. Nayfeh, D.T Mook, Nonlinear response of a taut string to longitudinal and transverse end excitation, *Journal of Vibration and Control* 1 (1995) 307–334.
[19] Y. Fujino, P. Warnitchai, B.M. Pacheco, An experimental and analytical study of autoparametric resonance in a 3DOF model of a cable-stayed-beam, *Nonlinear Dynamics* 4 (1993) 111–138.
[20] V. Gattulli, M. Lepidi, Nonlinear interactions in the planar dynamics of cable-stayed beam, *International Journal of Solids and Structures* 40 (2003) 4729–4748.
[21] V. Gattulli, M. Lepidi, J.H.G. Macdonald, C.A. Taylor, One-to-two global-local interaction in a cable-stayed beam observed through analytical, finite element and experimental models, *International Journal of Non-Linear Mechanics* 40 (2005) 571–588.
[22] C.T. Georgakis, J.H.G. Macdonald, C.A. Taylor, Non-linear analysis of wind-induced cable-deck interaction, *Proceedings IABSE Conference on Cable-supported Bridges: IABSE Reports* 84, Seoul, 2001, Paper 330.
[23] R. Lorenzo, Modelling of Cable-Structure Interaction in Cable-Stayed Bridges and Examination of their Parametric Response Under Stochastic Loading, PhD Thesis, University of Bristol, 2006.
[24] H.M. Irvine, T.K. Caughey, The linear theory of free vibrations of a suspended cable, *Proceedings of the Royal Society of London, Series A* 341 (1974) 299–315.
[25] A. Gonzalez-Buelga, S.A. Neild, D.J. Wagg, J.H.G. Macdonald, Modal stability of inclined cables subjected to vertical support excitation, *Journal of Sound and Vibration* 318 (3) (2008) 565–579.
[26] Y. Warnitchai, T. Fujino, A. Susumpov, A nonlinear dynamic model for cables and its application to a cable structure-system, *Journal of Sound and Vibration* 187 (4) (1995) 695–712.

[27] M.J. Ernst, Der E-Modul von Seilen unter Berücksichtigung des Derchhanges (The E-modulus of cables taking into account their sag), *Der Bauingenieur* 40 (2) (1965) 52–55 in German.
[28] T. Bakri, R. Nabergoj, A. Tonel, F. Verhulst, Parametric excitation in non-linear dynamics, *International Journal of Non-linear Mechanics* 39 (2004) 311–329.
[29] D.J. Wagg, S.A. Neild, in: *Nonlinear Vibration with Control*, Springer, 2010.
[30] F. Verhulst, in: *Nonlinear Differential Equations and Dynamical Systems*, Springer, 1996.
[31] A. Tondl, T. Ruijgrok, F. Verhulst, R. Nabergoj, in: *Autoparametric Resonance in Mechanical Systems*, Cambridge University Press, 2000.
[32] A.H. Nayfeh, D.T Mook, in: *Nonlinear Oscillations*, Wiley, 1979.
[33] V. Gattulli, M. Lepidi, Localization and veering in the dynamics of cable-stayed bridges, *Computers and Structures* 85 (21-22) (2007) 1661–1668.
[34] E. Caetano, A. Cunha, V. Gattulli, M. Lepidi, Cable-deck dynamic interactions at the International Guadiana Bridge: on-site measurements and finite element modelling, *Structural Control and Health Monitoring* 15 (2008) 237–264.
[35] W.E. Daniell, J.H.G. Macdonald, Improved finite element modelling of a cable-stayed bridge through systematic manual tuning, *Engineering Structures* 29 (3) (2007) 358–371.
[36] J.H.G. Macdonald, C.A. Taylor, B.T. Thomas, E.L. Dagless, Real time remote monitoring of dynamic displacements by computer vision, *Proceedings of the Sixth Society for Earthquake and Civil Engineering Dynamics Conference*, Oxford, 1998, pp. 389–396.
[37] J.H.G. Macdonald, Separation of the contributions of aerodynamic and structural damping in vibrations of inclined cables, *Journal of Wind Engineering and Industrial Aerodynamics* 90 (1) (2002) 19–39.
[38] F. Benedettini, G. Rega, Planar nonlinear oscillations of elastic cables under superharmonic resonance conditions, *Journal of Sound and Vibration* 132 (1989) 353–366.
[39] S.R.K. Nielsen, P.H. Kirkegaard, Super and combinatorial harmonic response of flexible elastic cables with small sag, *Journal of Sound and Vibration* 251 (1) (2002) 79–102.
[40] C.S. Hsu, W.H. Cheng, Steady-state response of a dynamical system under combined parametric and forcing excitations, *ASME Transactions: Journal of Applied Mechanics* 41 (2) (1974) 371–378.
[41] H. Troger, C.S. Hsu, Response of a nonlinear-system under combined parametric and forcing excitation, *ASME Transactions: Journal of Applied Mechanics* 44 (1) (1977) 179–181.
[42] N. HaQuang, D.T. Mook, R.H. Plaut, Non-linear structural vibrations under combined parametric and external excitations, *Journal of Sound and Vibration* 118 (2) (1987) 291–306.